INSTITUTE OF PHYSICS PUBLISHING and INTERNATIONAL ATOMIC ENERGY AGENCY NUCLEAR FUSION

Nucl. Fusion **42** (2002) 388–402 PII: S0029-5515(02)35450-4

Optimization of pellet scenarios for long pulse fuelling to high densities at JET*

P.T. Lang[1], B. Alper[2], L.R. Baylor[3], M. Beurskens[4], J.G. Cordey[2], R. Dux[1], R. Felton[2], L. Garzotti[5], G. Haas[1], L.D. Horton[1], S. Jachmich[6], T.T.C. Jones[2], P.J. Lomas[2], A. Lorenz[1], M. Maraschek[1], H.W. Müller[1], J. Ongena[6], J. Rapp[7], M. Reich[8], K.F. Renk[8], R. Sartori[9], G. Schmidt[10], M. Stamp[2], W. Suttrop[1], E. Villedieu[2], EFDA–JET Work Programme Collaborators[a]

[1] Max-Planck-Institut für Plasmaphysik, Euratom Association, Garching, Germany
[2] Euratom–UKAEA Fusion Association, Culham, Abingdon, Oxfordshire, United Kingdom
[3] Oak Ridge National Laboratory, Oak Ridge, TN, USA
[4] FOM Instituut voor Plasmafysica Rijnhuizen, Nieuwegein, Netherlands
[5] Consorzio RFX, Associazione Euratom–ENEA sulla Fusione, Padua, Italy
[6] Laboratory for Plasma Physics, ERM/KMS, Association Euratom–Belgian State, Brussels, Belgium
[7] Institut für Plasmaphysik, Forschungszentrum Jülich GmbH, Jülich, Germany
[8] Institut für Experimentelle und Angewandte Physik, Universität Regensburg, Regensburg, Germany
[9] European Fusion Development Agreement Close Support Unit, Garching, Germany
[10] Princeton Plasma Physics Laboratory, Princeton University, Princeton, NJ, USA

E-mail: ptl@ipp.mpg.de

Received 18 June 2001, accepted for publication 29 October 2001
Published 22 April 2002
Online at stacks.iop.org/NF/42/388

Abstract
Pellet injection was investigated for its fuelling capability to high densities in ELMy H mode discharges at JET. Applying the high field side launch system, optimized refuelling scenarios were developed on the basis of conventional discharge configurations with $I_p = 2.5$ MA, $B_t = 2.4$ T, averaged triangularity $\langle\delta\rangle \approx 0.34$ and mainly neutral beam heating at a level of approximately 17 MW. The accessible operational range was extended with respect to gas puff refuelling by the use of pellet injection. For example, H mode conditions could be maintained at densities beyond the Greenwald level. Plasma energy confinement was observed to become density independent at high densities. Deep pellet particle deposition made possible the uncoupling of edge and core density, allowing more peaked density profiles. When confinement deterioration due to pellet triggered MHD activity or parasitic pellet borne gas was avoided in appropriate pulse schedules, an enhanced particle inventory was achieved while maintaining the plasma pressure profile. In a technical assessment it was found that there is still room for further enhancement of the injection scenario by improved adaptation to high density plasma operation.

PACS number: 52.50.-b

1. Introduction

ITER-FEAT, planned to be the first fusion experimental reactor operating for research in physics and engineering, has been designed to satisfy specific technical requirements but also to have flexibility of plasma operation for studying burning plasma and for the optimization of plasma performance for various objectives. Requirements for the plasma performance are: extended burn in inductively driven plasmas at energy gain $Q > 10$; demonstration of steady state operation through current drive at $Q > 5$; and controlled ignition not precluded [1,2]. Operation scenarios [3] are based on the ELMy H mode because of its reproducibility and robustness, as well as its demonstrated long pulse capability and a well established database.

The development of plasma pulses in the inductively driven regime aims at a gradual increase of fusion power and

* Work performed under the European Fusion Development Agreement.
[a] See the Appendix of Pamela, J., JET–EFDA Team, in Fusion Energy 2000 (Proc. 18th Int. Conf. Sorrento, 2000), IAEA, Vienna (2001) CD-ROM file PD/1 and http://www.iaea.org/programmes/ripc/physics/fec2000/html/node1.htm.

plasma density with a typical density of $0.85 \times \bar{n}_e^{GW}$ (with $\bar{n}_e^{GW}$ the Greenwald density [4]) while achieving $Q = 10$ at a fusion power of 400 MW. If necessary, high fusion power operation at up to 700 MW at an even higher density level will be applied. Typical discharge parameters for the very long pulse lengths of about 1000 s needed to achieve thermal steady state operation will yield a density of $0.92 \times \bar{n}_e^{GW}$. In this regime, modes that are improved beyond the conventional ELMy H mode will eventually have to be explored. One possible candidate is a weak negative or shallow shear profile with an internal transport barrier at about 3/4 of the minor radius a_0, making fuelling beyond this transport barrier desirable in order to obtain a density profile which increases the bootstrap current. Therefore the option to use efficient pellet injection to achieve higher fusion power or to allow the favourable modification of the density profile has significant potential to improve operational flexibility.

For this reason, investigations regarding pellet refuelling and considerations of technological feasibility have been conducted at the Joint European Torus (JET) under the European Fusion Development Agreement (EFDA) framework collaboration. Experimental studies concentrating on aspects of efficient particle replenishment and refuelling scenarios were undertaken. Experiments started with conventional, well established ELMy H mode scenarios, with easy to handle plasma configurations and control sequences. A broad database for similar refuelling experiments with ordinary gas puff refuelling is available. On the basis of these reference discharges, scenarios were developed for long pulse fuelling to high densities in the vicinity of the Greenwald density while conserving the plasma energy to a maximum extent and keeping the impurity level low. For the experiments, the new pellet injection system using in-vessel guide tubes was employed, allowing pellet launch from both the torus low field side (LFS) and high field side (HFS).

In this article, results of the experimental investigations are reported along with consideration of their impact on the layout for a further optimized pellet launch set-up. Requirements and different options to enhance pellet refuelling performance beyond the status already achieved are presented. Also, a possible solution for a straightforward improvement of the currently installed HFS launch scheme is discussed.

2. Pellet refuelling physics

2.1. Impact of the injection scheme on refuelling performance

The injection of solid pellets produced from hydrogen isotopes for particle replenishment in a plasma discharge instead of gas bleeding was initially foreseen to produce more favourable particle deposition profiles deeper inside the plasma column. The advantages of pellet injection were even expected to increase with the size and temperature of the plasma. Whereas the fraction of gas particles able to cross the last closed flux surface strongly decreases, pellet ablation outside the separatrix remains negligible. Pellets can penetrate rather deep even into auxiliary heated plasmas. In the plasma, a spherical neutral cloud forming around the pellet [5] protects the pellet against incoming heat flux. Strong additional shielding results from partly ionized ablated particles spreading along magnetic field lines. This expanding plasmoid causes a cooling of the plasma in the flux tubes around the pellet [6]. Indeed, fuelling efficiencies ϵ (pellet induced plasma particle inventory increase N_e/pellet particle inventory N_P) close to unity were found. Improved confinement after pellet injection was also realized in experiments performed in ohmic plasmas [6, 7].

However, with the standard injection scheme from the torus outer side a rapid decrease in fuelling efficiency as well as a growing shift of ablated particles towards the plasma edge were found with increased heating power [8], reducing the pellet advantage with respect to gas puffing. The origin of this behaviour was identified as the curvature drift acting in a tokamak's inhomogeneous magnetic field on the ablation plasmoid [9–11]. In a hot plasma with pellet injection from the torus outside, chosen for its technical simplicity, the ablation cloud forms a plasmoid with high internal pressure which is subject to a strong drift force directed to the magnetic LFS, causing the observed outward motion. Advantage was taken of this situation by applying inboard pellet launch, where both the pellet velocity and the drift force are directed towards the plasma centre. The very first proof of principle experiment already showed that in comparable target plasmas with sufficient heating power the fuelling efficiencies realized with HFS pellet injection can far surpass equivalent values obtained for LFS launch [12]. Moreover, further experiments showed HFS injection to be more suitable for refuelling purposes than LFS launch despite launch speed restrictions imposed by the need for the pellets to be guided through tubes [13, 14]. The analysis of experiments performed at different tokamaks with an HFS injection path tilted from the horizontal plane seems to indicate that the advantages of the inboard launch are due not only to an inward shift of the initial particle source profile but also to deeper pellet penetration. Obviously, a strong influence on the ablation process is imposed by the drift force acting on the ablation plasmoid. Ejection of the plasmoid to the LFS occurring discontinuously causes strong ablation rate fluctuations, showing up as 'striations' in radiation emitted during pellet ablation [15]. This results in a precooling of the plasma ahead of the pellet and a reduction of the ablation rate for a pellet launched from the HFS. An LFS pellet, however, loses its plasmoid shield by this stripping process and is therefore subject to an enhanced thermal flux into the neutral cloud which increases the ablation rate.

Both injection schemes seem to follow the same parameter dependences for the pellet penetration depth λ_P, which depends on plasma parameters such as density and temperature but also on pellet mass m_P and velocity v_P. However, in typical refuelling experiments HFS pellet injection doubles the penetration depths achieved with LFS launch [16, 17]. As $\lambda_P \sim v_P^{1/3}$, this penetration depth doubling corresponds to an increase of the launch speed by a factor of 8, not taking into account the deposition profile shift, which increases the HFS improvement further.

Even more advantage is gained by HFS injection in H mode plasmas. With its critical edge pressure gradient, the H mode is very sensitive to shallow particle deposition. Depositing large amounts of cold particles close to the edge causes strong pressure flux into this region, finally resulting in the release of strong ELM activity expelling most of the deposited particles from the plasma. Since particle transport

causes fast particle escape from the plasma column in any case, shallow particle deposition becomes even more troublesome in H mode discharges. LFS pellet injection, with its tendency for shallow particle deposition in hot plasmas, hampers the refuelling performance severely. The advantages of the HFS injection technique, especially for refuelling H mode plasmas, made it the first choice for almost all experiments aiming at reactor relevant conditions.

2.2. Measures for the refuelling performance

A pellet injected into a plasma ideally causes an adiabatic plasma particle inventory rise by the amount of the particles contained in the pellet. Provided the pellet triggers no mode transition in the target plasma, this density surplus starts decaying as the plasma returns into its initial state. The decay time τ_P of the pellet induced density enhancement should thereby equal or even surpass the background plasma's particle confinement time τ_0, while the plasma's stored energy is kept at the initial level W_0 or is even increased. The improvement of plasma performance, characterized by, for example, W_0 or τ_0, with increasing density is prescribed by most empirical confinement scalings derived from data obtained in medium to low density plasmas, which do not correctly represent the density scaling of the confinement in the high density regime. Usually experiments show confinement degradation when approaching the Greenwald density [18]

$$\bar{n}_e^{GW}\ (10^{20}\ \mathrm{m}^{-3}) \equiv \frac{I_p\ (\mathrm{MA})}{\pi a_0^2\ (\mathrm{m})} \tag{1}$$

with I_p the plasma current and a_0 the horizontal minor radius [4]. In reality the density enhancement is only a fraction ϵ of the pellet mass and usually the effective decay time $\tau_P < \tau_0$. Both ϵ and τ_P are useful figures of merit for the refuelling performance achieved.

Assuming a steady state background plasma with base density $\bar{n}_e^b$ where each single pellet causes a density increase $\bar{n}_P$, the injection of a continuous pellet string with a temporal pellet distance t_P causes a step by step density ramp-up until stagnation at a density enhancement level Δ is reached. Every further pellet then causes an increase towards a peak density $\bar{n}_e^b + \Delta + \bar{n}_P$, decaying to $\bar{n}_e^b + \Delta$ just before the next injection. From the stagnation condition

$$(\Delta + \bar{n}_P) e^{\frac{-t_P}{\tau_P}} = \Delta \tag{2}$$

the steady state density enhancement can be calculated as

$$\Delta = \frac{\bar{n}_P}{e^{\frac{t_P}{\tau_P}} - 1}. \tag{3}$$

This simplified picture shows that the pellet induced density enhancement can be tuned by modifying one or more of the three parameters single pellet density hub, pellet repetition rate and density relaxation time.

In a real refuelling experiment, t_P is predetermined and is often imposed by technical limitations of the injection system. The processes occurring during pellet ablation, particle deposition and further density profile evolution can be subdivided into different phases evolving on different timescales. The fastest timescale is connected with the curvature drift acting on the high beta ablation plasmoid. This process can cause dislocation of the ablated material over several centimetres within only microseconds, rearranging the ablation profile with respect to the deposition profile even while the ablation of the pellet, which typically lasts for about 1 ms, is still in progress. Thus significant loss of ablated particles out of the plasma can take place on a submillisecond timescale, before equilibration on a flux surface is established and too fast for the temporal resolution of standard particle inventory measurements. Values obtained for the pellet induced density enhancement thus usually consider losses picked up by the curvature drift and take these into account by the experimental value of $\epsilon = N_e/N_P$, with N_e measured a few milliseconds after pellet injection. Fuelling efficiencies obtained this way show higher values when deeper particle deposition is achieved, for example by HFS launch, due to the reduction of particle losses during the transition from ablation to deposition profile.

Once the pellet has burnt out and the fast drift has settled, a deposition profile is established, usually forming a density profile with an off-axis density hump. Relaxation of this non-equilibrium profile towards the initial steady state profile then occurs on typical transport timescales. In the early phase of this diffusive relaxation, particles spread from the main deposition zone towards both the edge and the core plasma region while the pellet induced density hump starts broadening. This phase is characterized by a gradual increase of the central density n_{e0} and, since the strong perturbation of the density profile broadens and decreases, also by a gradual slowing down of the density decay rate. During this phase, the density profile achieves its maximum peakedness $n_{e0}/\bar{n}_e$. In the later phase of the density profile relaxation, the density decreases across the entire plasma radius and the decay time approaches τ_0.

This behaviour is shown in Fig. 1, where the typical evolution of the density profile (upper box) as well as those of the volume averaged density $\langle n_e \rangle$ and central density n_{e0} (lower box) are given. This example of profile evolution was calculated assuming a simple flat diffusion profile across the entire plasma column and a diffusivity typical for a JET plasma. It shows the diffusivity driven density decay starting with a decay time of 22 ms, and finally slowing down to about 160 ms. Transport analysis of the post-pellet particle transport showed diffusivity $D(r, t)$ varying both spatially and temporally. Moreover, inward pinch drift effects modify the picture quantitatively but not qualitatively. In the experiment, indeed, a significant slowing down of the density decay rate is often observed, usually characterized by a fast and a slow component [13, 19].

During H mode phases, strong rapid changes of the diffusivity in the edge transport barrier region marked by ELMs cause a more steplike $\bar{n}_e$ evolution. ELMs are correlated with strong particle losses while $\bar{n}_e$ stays essentially constant between ELMs. However, since ELM bursts only discontinuously expel particles stuck at the edge barrier, the density decay averaged over many ELM events again shows the general behaviour described before, and an averaged value of τ_P is still a useful figure of merit for the refuelling performance [20].

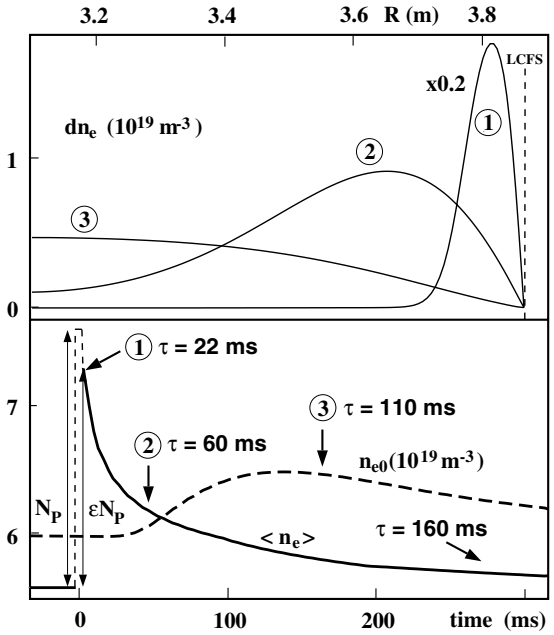

Figure 1. Radial profiles of the pellet induced density enhancement 1, 50 and 170 ms after pellet burn-out (upper box). Instant pellet particle losses are described by the fuelling efficiency ϵ, the decay of the pellet induced density increase slowing down while particles diffusing into the core plasma cause more density peakedness (lower box).

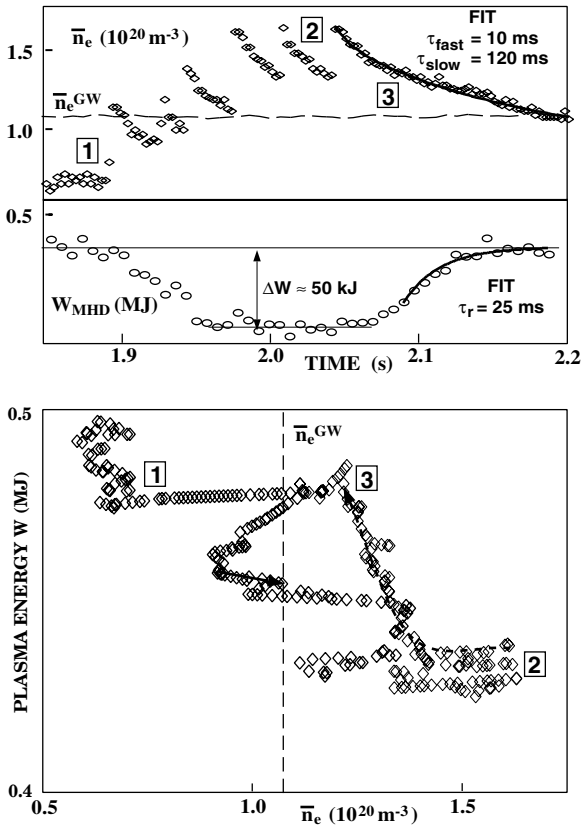

Figure 2. Upper box: $\bar{n}_e$ and plasma energy evolution during and after a pellet sequence. Lower box: fuelling cycle in the $\bar{n}_e$–W diagram for ASDEX Upgrade [13].

2.3. Pellet induced energy losses and pellet fuelling cycle

Particles lost during the diffusive post-pellet density decay phase are obviously already thermalized and thus also impose strong energy losses. This was concluded from the fact that confinement degradation was still encountered during quasi-steady-state pellet refuelling, i.e. an energy decrease at the same time as a density increase, even in the case when confinement reduction by, for example, strong mode activity or an excessive edge density increase, can be ruled out. The observed operational boundaries can be explained by introducing an assumed additional loss power in the power balance equation [21]. In this calculation, the initial relation $P_{heat} = P_{loss} = W_0/\tau_E$ (with P_{heat} and P_{loss} heating and loss power and τ_E the initial energy confinement time) is modified by the total additional losses $P_{dec} = 3\Phi_{dec}k_B\langle T\rangle$ caused by the pellet induced particle outflux Φ_{dec} from the plasma ($\langle T\rangle$: averaged plasma temperature in the deposition area).

As the energy reduction ΔW with respect to W_0 increases with Φ_{dec}, the strongest confinement reduction takes place in the early phase of diffusive density decay, characterized by the fast component and, in H mode phases, by strong pellet induced ELM activity. Much lower particle and energy losses take place in the later phase governed by the slow decay component. This is shown in Fig. 2, where the temporal evolution of plasma energy and $\bar{n}_e$ is plotted in the upper part for a sequence of six pellets and the density decay phase thereafter. In this experiment, performed at ASDEX Upgrade, nominal $(2\ \mathrm{mm})^3$ deuterium cubes were injected into a plasma heated by 5 MW neutral beam injection (NBI) [13].

A fit to the post-pellet $\bar{n}_e$ evolution yielded $\tau_{slow} = 120$ ms for the late and $\tau_{fast} = 10$ ms for the early component, in quite good agreement with $(d_P/a_0)^2 \times \tau_0 \approx (0.15\ \mathrm{m}/0.42\ \mathrm{m})^2 \times 120\ \mathrm{ms} = 15\ \mathrm{ms}$ estimated from the averaged deposition depths d_P. With the duration of the fast phase almost equal to $t_P = 1/30$ s, losses stay high throughout the complete pellet sequence. Here

$$\Delta W = \frac{P_{dec}}{P_{heat}} W_0 \approx 0.1 \times 0.5\ \mathrm{MJ} \qquad (4)$$

results in a significant plasma energy reduction while ΔW becomes negligible in the slow decay phase.

Indeed, this drastic reduction of the additional loss power in the slow decay phase allows a fast, almost complete recovery of the plasma energy to the initial value. Moreover, with the energy recovery time $\tau_r = 25$ ms being less than τ_{slow}, full initial confinement can be regained while the density level is still elevated. This is shown in the lower part of Fig. 2, where the evolution of this sequence is shown in an operational $\bar{n}_e$–W diagram. Obviously, enhanced operational conditions with respect to plasma energy and density can be realized transiently in the post-pellet phase.

Use was made of this combined density and confinement behaviour in the first pellet refuelling experiments at JET using the new HFS launch facility [14, 19]. Interruptions at the end of a long pellet sequence applied for steady state refuelling resulted in performance improvement. However, long pellet strings previously injected in these experiments had caused strong confinement reduction down to insufficient values. Therefore the guideline for long pulse refuelling

experiments to high densities reported here was to optimize the pellet refuelling sequence in order to prevent too drastic pellet induced energy losses. With the intention of achieving sufficient particle influx for density ramp-up but also of avoiding unsuitable loss power and thus confinement reduction, tailoring of the pulse and injection schedules was undertaken.

3. Experimental set-up and technical equipment

Experiments were performed at the European Atomic Energy Community's largest fusion project, JET, a tokamak with the essential objective of obtaining and studying plasmas in conditions and with dimensions approaching those needed in a thermonuclear reactor. JET is a non-circular divertor tokamak with a major plasma radius $R_0 = 2.96$ m and a minor radius $a_0 = 1.25$ m, operated during this campaign with the Mark II gas box divertor with central septum. Lower single null plasma configurations applied in this study typically had elongations $\kappa \approx 1.7$, volumes $V_p \approx 80$ m^3 and an edge safety factor $q_{95} \approx 3.2$ with a toroidal magnetic field $B_t = 2.4$ T and plasma current $I_p = 2.5$ MA, or $B_t = 2.7$ T and $I_p = 2.8$ MA. D shaped equilibria were run with averaged triangularity $\langle\delta\rangle \approx 0.34$ (upper triangularity $\delta^u \approx 0.38$, lower triangularity $\delta^l \approx 0.30$), referred to as the HT configuration, or with $\langle\delta\rangle \approx 0.25$ ($\delta^u \approx 0.24$, $\delta^l \approx 0.25$), referred to as the LT configuration. The two configurations were used both in the standard vertical (V) target version with the separatrix strike zone on the vertical divertor target plates and in a slightly modified 'corner' (C) version, where the outer strike zone was fitted deep into the pump throat towards the pumping slit in the corner of the divertor plates. Thus the effective pumping speed for the main chamber plasma applied by the toroidal cryopump (cooled by supercritical helium) installed behind the outer divertor vertical target plate was maximized. For auxiliary plasma heating, mainly NBI (D^0 injection) was used, with the beams operated at 80 kV (4 Oct.) and 120 kV (8 Oct.). A further increment of P_{heat} beyond the maximum available NBI power of about 17 MW took place in a few shots with additional ion cyclotron resonance heating (ICRH) of up to 3 MW with the fundamental hydrogen resonance on the axis (37.3 MHz at 2.4 T, 42.5 MHz at 2.7 T, all antennas with $-\pi/2$ phasing). Although the experiments were performed in deuterium plasmas, a few per cent of hydrogen was added to achieve better coupling of the ICRH when needed. The vacuum vessel was conditioned by a 4 h helium glow discharge cleaning and beryllium evaporation the night before and was baked to 320°C during operation.

The JET pellet injection system is based on a centrifuge pellet injector equipped with an extruder pellet source. This source is capable of delivering nominal (4 mm)^3 cubic D pellets (containing 3×10^{21} D atoms) at a maximum 10 Hz repetition rate. Pellet launch velocities are set by the centrifuge revolution frequency f_C to v_P (m/s) $= 3.1 \times f_C$ (Hz), and possible repetition rates are restricted to values f_C/n (n integer) by the centrifuge acceleration scheme. For the same reason, timing of the pellet launch is possible only with the accuracy of one centrifuge revolution period. Pellet size, velocity and repetition rate are bound to extruder and centrifuge settings and are thus fixed within one plasma discharge but are easily changed between subsequent shots. In order to prevent strong mass variations during a pellet sequence, a continuous train of typically 20 s duration is ejected. By means of a three way selector acting faster than 100 ms, every single pellet can be directed either to the guide tube for HFS or LFS launch or into a pellet dump. In this way, switching between LFS and HFS launch or shortening the repetition rate to a fraction of the preselected value can be done. A maximum pellet launch speed of 600 m/s can be reached by the accelerator; however, pellet fragmentation in the guide tubes causes restrictions on usable launch speeds. For horizontal LFS injection at the torus midplane, a maximum speed of 360 m/s can be achieved while maintaining good pellet reliability. With the current HFS launch set-up, pellets are not aimed at the plasma centre but are tilted by 44° to the horizontal plane with a tangency radius at a normalized minor radius of $\rho \approx 0.6$–0.7 in typical configurations. This scheme was chosen to maximize the radius of curvature at the exit of the in-vessel guide tube to $R_c = 220$ mm, with usable launch speeds nevertheless limited to 160 m/s. A schematic poloidal cross-section of JET including the magnetic flux tube pattern of an HT–C configuration is given in Fig. 3. Also included are the injection paths for the LFS and HFS pellet launch.

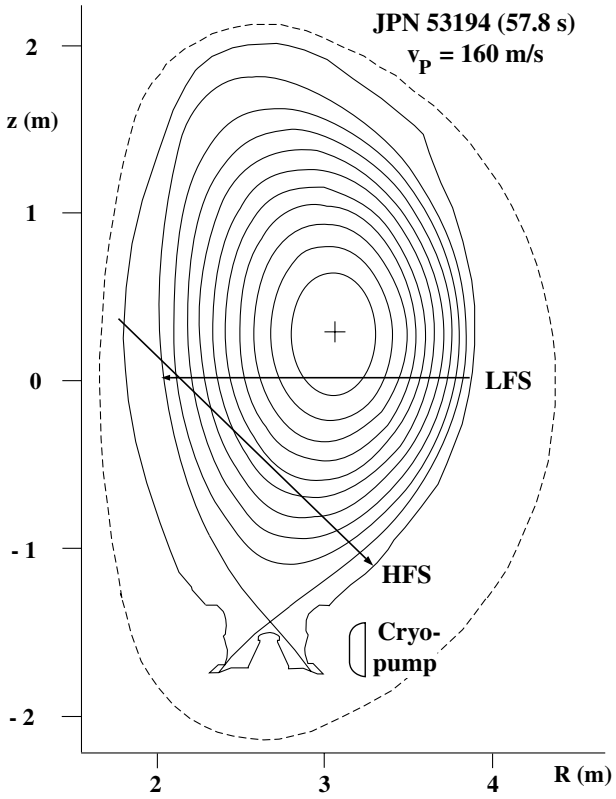

Figure 3. Poloidal cross-section of JET with the Mark II gas box divertor and central septum; magnetic structure of lower single null HT–C plasma configuration with $I_p = 2.5$ MA, $B_t = 2.4$ T, $q_{95} = 3.2$, $\langle\delta\rangle \approx 0.34$ and strike zone deep in the divertor throat for efficient pumping. The injection paths used for LFS (max. $v_P = 360$ m/s) and HFS (max. $v_P = 160$ m/s) launch are also shown.

For the investigations, use was made of the broad pool of diagnostic facilities provided at JET. Particular systems, e.g. the ablation radiation monitor or the fast magnetic signal

recording system, were set to record data sequences at high temporal resolution. The first pellet of the sequence was usually adjusted to the times when temperature and density profiles were taken by the core and edge LIDAR systems in order to be able to obtain useful particle deposition profiles shortly after the injection.

Since confinement degradation caused by excessive density ramp-up and plasma cooling eventually leads to a core radiation collapse, a real time control circuit algorithm was implemented to prevent further pellet injection. By this means, plasma disruptions caused by the pellet programme could be avoided most of the time.

4. Results

The intention of our investigations was to find a way of using pellet refuelling to obtain densities in the vicinity of $\bar{n}_e^{GW}$ while keeping the confined energy high. Using the available instrumentation and features, the concept was to improve performance by developing target plasma discharges fully compatible with pellet refuelling and by optimizing the adapted pellet sequences. Special attention was paid to the pellet fuelling cycle in order to obtain both maximum peak values and acceptable averaged performance parameters at the same time.

4.1. Direct comparison of LFS and HFS launch

The greater suitability of the available HFS launch scheme compared with LFS injection due to the improved performance parameters achieved with HFS in similar plasma configurations was tested and proven by direct comparison within a single discharge. For this scenario, the flat-top phase of an LT–V 2.5 MA/3.2 T discharge with constant $P_{heat} = 6.5$ MW (1.1 MW ohmic, 4.5 MW ICRH and 0.9 MW NBI) was chosen. At this heating power level, plasma temperature is already sufficient to allow the occurrence of significant curvature drift. On the other hand, quiescent L mode conditions are still kept. Avoiding the transition into H mode prevents ELM activity, keeping temporal plasma parameter evolutions smooth, allowing better analysis. $v_P = 158$ m/s and a pellet rate of 5.1 Hz were chosen as pellet parameters. At this repetition rate, density profiles were obtained by the LIDAR system operating at 4 Hz with a time delay gradually increasing with respect to pellet injection from pellet to pellet. Using this sampling technique, the relaxation of the deposition profiles could be observed.

Results obtained from this experiment are shown in Fig. 4. A continuous train of pellets with virtually constant mass at the centrifuge exit (measured by a microwave detector) was injected for more than 5 s duration, beginning with LFS launch. With density stagnation achieved at $\Delta_{LFS} = 2.2 \times 10^{19}$ m^{-3} in this scenario, the launch position was switched to the HFS after 3 s. As can be seen from the lower left part of Fig. 4, changing the launch scheme does not affect the plasma diamagnetic energy content but results in an increased line averaged ($\Delta_{HFS} = 3.3 \times 10^{19}$ m^{-3}) and central density as well as in more peakedness. Profiles plotted in the upper part of Fig. 4, obtained in the density stagnation phase immediately after (left) or just before (right) another pellet, show that

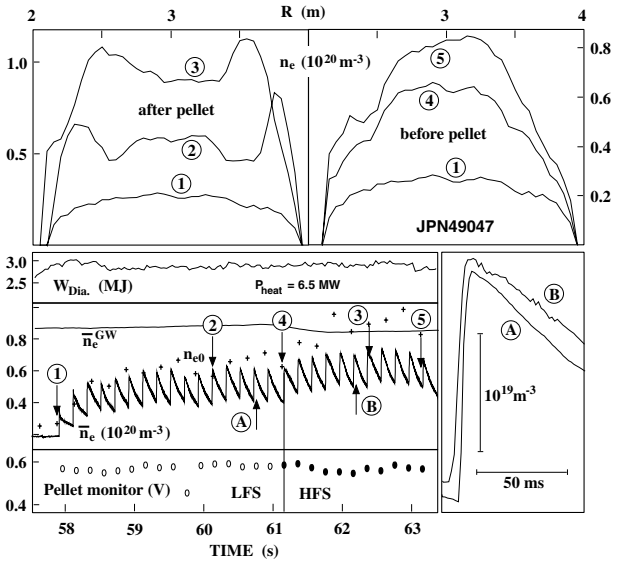

Figure 4. Comparison of LFS and HFS injection in a single plasma discharge. Lower left: Injection of a train of almost equally sized pellets (signal from a microwave monitor) first from the LFS (A; bottom, open circles) and then from the HFS (B; bottom, filled circles) into an L mode plasma. A switch to HFS launch causes an increase of $\bar{n}_e$ (signal sampling time 1 ms) and n_{e0} beyond the LFS level (middle), while plasma energy remains unchanged (top). Upper box: Density profiles taken immediately after pellet injection (left) show deeper particle penetration, while profiles taken before the next pellet (right) show more peakedness and density elevation across the entire plasma cross-section in the case of HFS launch. Numbers against the density profile evolution traces correspond to the numbers on the density curve in the lower left part of the figure. Lower right: Density decay after pellet injection. A and B correspond to LFS and HFS launch, respectively.

HFS pellets deposit particles deeper inside the plasma, thus eventually driving density to higher values across the entire plasma cross-section. Moreover, slightly slower density decay is achieved with HFS pellets, shown in the lower right part of Fig. 4, where the $\bar{n}_e$ evolution after pellet injection is compared for typical HFS and LFS pellets on an expanded timescale.

The advantage of HFS over LFS injection became quite clear in this experiment despite the still rather low heating power applied and the less favourable geometry of HFS injection. Pellets transferred to the HFS must pass through a significantly longer guide tube with unfavourable curvature, thus arriving at the plasma with about 1/3 less mass than pellets transferred to the LFS. Moreover, the effective injection speed $v_\perp \leqslant \cos(44^\circ) \times 158$ m/s $= 114$ m/s is lower. On the other hand, higher plasma density and reduced temperature for the HFS pellets somewhat compensate for these disadvantages. Estimating ablation depths for typical pellets injected during the density stagnation phases by applying the NGS model based IPADBASE scaling for JET [22] yielded values of 26 cm for the LFS and 25 cm for the HFS. Obviously, deeper pellet particle deposition (deposition depths $d_P^{HFS} \approx 60$ cm $> d_P^{LFS} \approx 35$ cm) is caused especially in the case of HFS injection by the curvature drift. Moreover, since essentially equal values $\bar{n}_P \approx 2 \times 10^{19}$ m^{-3} are obtained in both launch schemes, higher HFS fuelling efficiency easily balances the reduced m_P. The observed deeper particle deposition results, as expected, in a slowing down of the following density decay.

Applying Eq. (3), effective decay times of $\tau_P^{LFS} = 320$ ms and $\tau_P^{HFS} = 430$ ms can be calculated, in fairly good agreement with the values of 400 ms and 450 ms obtained in a direct fit of the $\bar{n}_e$ traces. (It should be noted that since the heating power in this experiment was quite low, and pellet penetration and particle deposition therefore deep, derived effective decay times were dominated by the slow final decay time.) However, it seems that the difference between τ_P^{LFS} and τ_P^{HFS} cannot be explained by the penetration depths alone, because the ratio of squared penetration depths is smaller than the ratio $\tau_P^{LFS}/\tau_P^{HFS}$. This might be due to a transient change of D in the post-pellet phase, as can be concluded from particle transport modelling results [23].Values for the fast onset of the density decay do not yet differ much from the value of 570 ms for the slow component, obtained by fitting the $\bar{n}_e$ decay to $\bar{n}_e^b$ after the pellet sequence. Therefore additional power losses imposed during the fast decay phase remain limited to negligible levels that it is not possible to resolve by the plasma energy content measurement. This comfortable situation becomes less favourable rather quickly with increasing heating power, and penetration and deposition depths are significantly reduced for both HFS and LFS pellets. However, degradation of fuelling efficiency and fast density decay time are much more severe in the LFS case, making HFS launch even more advantageous at higher power levels [24]. Therefore, from the fact that HFS injection shows better fuelling performance even at the moderate P_{heat} level applied in this experiment, it can be concluded that applying HFS injection is advantageous also at all higher power levels and especially at levels beyond the H mode threshold. Consequently the available HFS injection facility was employed exclusively for further refuelling studies in the H mode regime.

4.2. Comparison of different discharge configurations with respect to their compatibility with pellet refuelling

Utilizing already well established JET pulse forms and employing HFS pellet injection, the initial task for achieving advanced global performance by means of pellet refuelling was to identify the most suitable target plasma conditions. Taking into account experience from a similar study performed at the mid-size tokamak ASDEX Upgrade [13], attention had to be directed to three critical issues:

— Prompt particle losses causing too strong an increase of neutral gas pressure and edge density;
— Triggering of mode activity by the pellet;
— ELM bursts following pellet injection.

Each of these pellet related effects can cause severe energy losses and must therefore be avoided or minimized. Their roles in a large tokamak were also investigated in detail.

4.2.1. Pellet impact on neutral gas density It is well known that H mode discharges undergo strong confinement degradation with increasing edge density, represented, for example, by the separatrix density n_e^{sep}. Further, a strong correlation exists between n_e^{sep} and the neutral gas density n_0. Increasing n_0, for example by gas puffing or strong particle release from the walls, drives up n_e^{sep} as well, eventually resulting in a significant reduction of the plasma energy content. For pellet refuelling, this can cause severe performance restrictions in the event that the parasitic pellet borne gas puff recycling at the wall induces too strong increases of n_0. Avoidance of this deleterious effect requires sufficient pumping capability to get rid of the parasitic pellet borne gas puff and prevent successive edge density ramp-up during the pellet sequence. As the maximum available pumping capability is limited in the experiment, it is necessary to restrict the applied pellet particle flux to values the pumping system can still cope with. Compatible values had to be derived for the minimum tolerable t_P for both the vertical and the corner configuration with the expected improved pumping properties. To perform this analysis and to have a means of monitoring the proximity of the discharge to the onset of confinement degradation, we employed the main chamber pressure measured by a Penning gauge installed at the torus midplane. This gauge signal, p_0^m, was chosen because of its high reliability and good signal to noise ratio. In the pressure range $p_0^m > 10^{-3}$ Pa in which we operated, there is a linear correlation between midplane and divertor pressure [25, 26]:

$$p_0^{div} = 154 \times p_0^m. \tag{5}$$

In reference discharges without gas or pellet particle fuelling, a neutral gas background in the range $p_0^m = (0.9\text{–}1.3) \times 10^{-3}$ Pa was found. Applying pellet rates of up to 6.25 Hz without additional gas puffing in appropriate plasma configurations results in an increase of the neutral gas pressure to a maximum of $p_0^m = 1.8 \times 10^{-3}$ Pa. From the temporal p_0^m evolution in shots with a very low pellet repetition rate, a relation between applied pellet particle flux and neutral gas pressure increase of

$$\frac{dp_0^m}{N_P} = (1.5 \pm 0.2) \times 10^{-25} \text{ Pa/D atom} \tag{6}$$

was derived. Of course, as pellet particles only gradually leave the plasma and equilibration and thermalization take place, the maximum in the arriving pressure pulse is delayed by typically about 150 ms with respect to pellet injection. This can be seen in Fig. 5, where density and pressure evolutions are displayed. They were achieved during low repetition pellet phases using the vertical or the corner configuration. As also shown in Fig. 5, a pressure pump-down rate of 1.6×10^{-3} Pa s^{-1} was found for the vertical configuration. Indeed, as expected, the corner configuration showed improved particle removal capability. A value of 3.0×10^{-3} Pa s^{-1} achieved in this configuration indicates an almost doubled particle removal capability, at least for the parasitic pellet borne gas puff. With a typical pellet particle inventory of $N_P = 1.6 \times 10^{21}$ D atoms found in the refuelling experiments, removing a single pellet's parasitic gas puff takes about 80 ms in the corner and 150 ms in the vertical configuration. From this consideration, tolerable pellet rates of about 12 and 7 Hz can be estimated for corner and vertical configurations, respectively.

A standard value for a tolerable parasitic gas puff level can also be obtained from an estimate of the gas flux in a steady state discharge without gas puff or pellet injection. Assuming an effective pumping speed for the divertor region of $S_{eff}^{div} = 160\,\text{m}^3/\text{s}$ and an equilibrium pressure of $p_0^m \approx 10^{-3}$ Pa,

$$\Phi = S_{eff}^{div} \times n_0^{div} \approx 9 \times 10^{21} \text{ s}^{-1}. \tag{7}$$

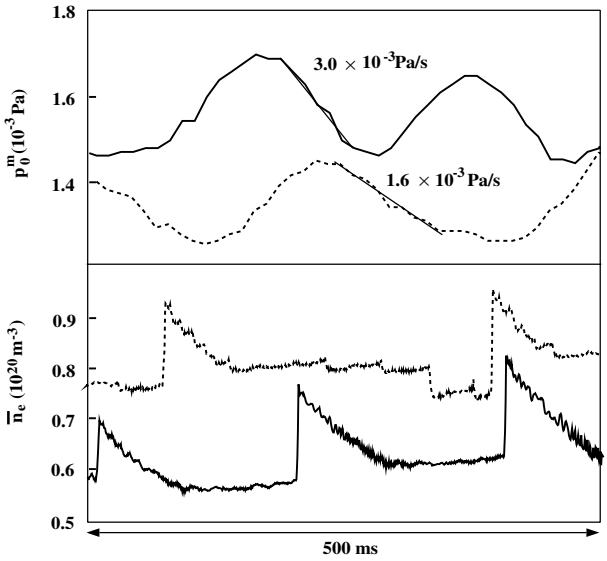

Figure 5. Midplane neutral pressure excursion (upper box) induced by additional particle fluxes from the plasma after pellet injection (indicated by the decaying line averaged density, lower box). In the corner configuration (solid curves), particles are removed at about twice the rate achieved with the vertical configuration (dashed curves).

With an NBI fuelling rate component of up to about 1.2×10^{21} s^{-1} only, this flux, mainly due to particle release from the wall reservoir, is equivalent to a pellet particle flux of about 6 Hz. High density refuelling approaches performed with the same plasma configuration by gas puffing at different levels showed that even somewhat larger particle fluxes can be tolerated. Significant confinement degradation only set in at gas puff rates exceeding 2×10^{22} s^{-1}, causing an increase of n_0^m beyond a critical value of 2×10^{-3} Pa.

Therefore it can be concluded that, with the available pellet size and pumping capacity, pellet repetition rates of up to about 7–10 Hz are still tolerable. Using the corner configuration for improved pumping, even more latitude for the repetition rate can be gained. With a maximum repetition rate of 6.25 Hz and a p_0^m value of 2×10^{-3} Pa, the danger of confinement degradation induced by excessive edge density and neutral pressure increase can be excluded. A significant influence on the plasma confinement by the parasitic pellet borne gas can thus be disregarded.

4.2.2. Pellet related core MHD mode activity MHD mode activity often limits the achievable performance in tokamak plasmas. Especially neoclassical tearing modes (NTMs) on resonant flux surfaces, driven by a helical hole in the bootstrap current resulting from the pressure flattening across magnetic islands, create a major problem for reaching high β values. In pellet refuelling scenarios, too, NTMs were found to threaten high performance [13]. Pellets driving up density thereby reduce the temperature. Reduction of the ion temperature causes a shrinking poloidal ion gyroradius $\rho^*_{p,i}$. According to the ion polarization current model, this reduces the critical pressure β_p^{onset} for the triggering of an NTM by a perturbation, since $\beta_p^{onset} \sim \rho^*_{p,i}$ holds [27]. Thus, if previous pellets have already driven down the plasma temperature too far, strong local perturbations on resonant surfaces introduced by a further pellet can trigger an NTM.

The mechanism of plasma cooling by the pellets finally resulting in the release of strong MHD activity which causes drastic confinement loss can be seen in Fig. 6. However, as can also be concluded from this discharge, confinement recovery can be effected by raising the temperature again. In the experiment displayed in Fig. 6, a continuous 5 s pellet string was injected at 5 Hz into a 2.4 MA/2.5 T C–HT plasma with 15–17 MW NBI heating. The first pellets arrived in a plasma showing good confinement and at the same time high W and β values, and the pellets drove up $\bar{n}_e$ while the energy remained almost constant (the slight reduction due to pellet induced ELM bursts is discussed in Section 4.2.3). With the plasma temperature reduced, $\rho^*_{p,i}$ was also reduced, and the plasma became more prone to MHD onset, which was finally triggered by the seventh pellet. Growing amplitudes of MHD modes caused a strong increase in particle and energy transport, resulting in a drastic reduction of particle and energy contents despite ongoing heating and refuelling. With the reduction of density being relatively stronger than the energy reduction ($\bar{n}_e$ decreased from 8×10^{19} m^{-3} to 4×10^{19} m^{-3} and W_{Dia} from 6 to 4.5 MW), the temperature even recovered slightly during this first confinement collapse phase. Higher temperatures and lower densities obviously allow confinement recovery as soon as the modes disappear. In the following phase the energy content was almost re-established to the initial level while the density again approached the Greenwald level. Because again conditions of high particle content but rather low temperature were reached, mode activity set in and another confinement collapse cycle started, once more followed by a recovery phase. The chosen plasma configuration with refuelling and heating at the levels applied here obviously cannot yield a stable scenario, as the discharge started to oscillate between two unstable configurations. Detailed analysis showed that it was mostly NTMs with (3/2) structure that caused confinement losses, but (4/3) and (2/1) modes also occurred. Moreover, during the pellet sequences, even (1/1) activity was sometimes detected. Different modes released by the pellets were also found in the example shown. Whereas several components, including a strong (1/1) share, caused the first confinement collapse, the second collapse stemmed from an almost pure (3/2) NTM.

To improve the situation with respect to NTMs, it is obviously necessary to keep the temperature above a critical level. Aiming at a density level in the vicinity of $\bar{n}_e^{GW}$, our prime choice to achieve this task was to increase the heating power. However, since only about $W \sim P^{0.34}$ is achieved in the ELMy H mode [28], quite meagre improvement, $\beta_p^{onset} \sim P^{0.17}$, is to be expected from this means. Nevertheless, plasmas with almost the same parameters as the discharge shown in Fig. 6 often showed much improved performance with P_{heat} increased by only a few megawatts. Achieving a drastic reduction of MHD activity by only moderately improved heating indicates that operating conditions achieved with the maximum P_{heat} applied in these experiments are close to the critical onset level of the modes.

Another way tried in the experiments to avoid NTMs at a given power level was to reduce the normalized plasma pressure β_N by increasing B_t. Indeed, discharges at elevated B_t seemed to be less plagued by core MHD activity. However,

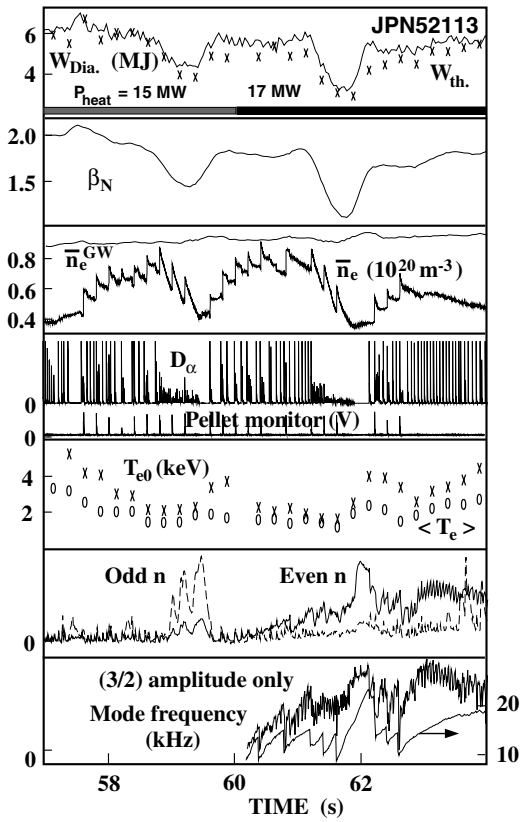

Figure 6. Pellet induced confinement oscillations. Density ramp-up causes gradual temperature reduction, resulting in strong MHD activity and a transient confinement collapse. Temperature recovery forces vanishing mode activity and confinement recovery, driving the discharge back to the high density, low temperature conditions prone to NTM onset. Detailed mode analysis shows that NTM activity can be composed of different modes during each confinement oscillation.

as they were hampered by enhanced ELM activity reducing the plasma performance, it cannot be concluded without doubt that increasing B_t is favourable for NTM suppression.

4.2.3. Pellet triggered ELM bursts The effect of pellet induced ELM bursts on the confinement has already been discussed in Section 2.3. Contrary to the effects of edge density and core MHD induced confinement deterioration, this degradation mechanism cannot be avoided completely by choosing suitable target plasma configurations. Therefore special emphasis must be placed on a proper minimization strategy for the ELM bursts. The most promising approach for this purpose is a reduction of the pellet rate to the lowest possible value that can maintain density at the required level but that also reduces energy losses. This can be achieved by tailoring the pellet sequence, as discussed in Section 4.2.4, and by choosing the most appropriate target discharge parameters. In particular we investigated the influence of I_p/B_t variations at a constant q_{95} on the pellet induced ELM losses. As a reduction of B_t was prevented by core MHD activity, target plasmas at 2.8 MA/2.7 T instead of 2.5 MA/2.4 T were tested.

A comparison of two similar discharges with these I_p/B_t values and approximately 15 MW NBI heating is presented in Fig. 7, which clearly shows a much less favourable behaviour with respect to pellet triggered ELMs at higher B_t. However, triggered by the fourth pellet, the low B_t shot develops a (3/2) NTM terminating the high performance, while no significant core MHD confinement reduction is found at higher B_t. Therefore only ELM loss dominated phases can be considered. Obviously there is a different ELM behaviour present. A few strong type I ELMs correlated with abrupt particle losses take place after pellet injection in the low B_t case.

In the high B_t discharge a gradual density reduction results from bursts of ELMs showing the typical type III characteristics of mild but frequent events. Overall, stronger averaged particle and energy losses take place for the higher ELM frequency, as indicated by the dashed lines in Fig. 7. Despite a somewhat higher pellet rate applied at 2.7 T (6.25 Hz; 5 Hz at 2.4 T), only about half the density ramp-up rate can be realized. Higher particle loss rates in the post-pellet phase require an enhanced pellet particle flux consumption to approach $\bar{n}_e^{GW}$ (in any case at a somewhat elevated absolute level owing to the higher I_p). A lower efficiency of fuelling at 2.7 T is shown, for instance, by a 0.26 fraction of injected particles still contained in the plasma when $\bar{n}_e^{GW}$ is reached with the tenth pellet. For the 2.4 T discharge, this is already achieved by the fifth pellet with 0.49 times the injected particles still present in the plasma. Stronger particle loss flux from the plasma also carries away more energy, yielding an averaged loss power of 1.1 MW compared with a reference value of 0.8 MW. However, a reduced averaged particle sustainment time somewhat reduces energy losses per particle ($\langle T \rangle$ of about 400 eV compared with 500 eV), mitigating convective energy losses. Stronger particle losses also result in enhanced parasitic pellet borne gas puffs. In the late phase of the pellet sequence, p_0^m rises beyond the critical pressure level, and edge density induced confinement deterioration begins.

The reason for this different behaviour might be the unfavourable scaling of the power threshold for type III ELMs with B_t. At the heating power applied, obviously the threshold for maintaining type I ELMs can no longer be surpassed once density increase and edge temperature reduction [29] by the pellets begin. The transition from the type I to the type III ELM regime is associated with a stronger reduction of the plasma energy content [18].

4.2.4. Optimizing the refuelling configuration To choose the best possible target plasma configuration for the final refuelling experiments, the following key elements had to be taken into account. Core MHD induced degradation, especially by pellet triggered NTMs, worsens with declining B_t, and the minimum value to operate in a well established pulse schedule within the heating power range at our disposal was 2.4 T. Pellet induced ELM losses were found to increase drastically with B_t; even using an alternative schedule at 2.7 T requires a doubled pellet particle flux to reach $\bar{n}_e^{GW}$. Higher particle losses result in stronger convective energy losses and eventually also in edge density induced confinement deterioration. It was therefore decided to operate at $B_t = 2.4$ T and at maximum P_{heat}. Auxiliary heating was based on NBI for its potential to provide heating for long periods at a constant and high power level. To supplement the NBI power resources, central ICRH was chosen despite the fact that power coupling into the plasma was troublesome and somewhat erratic in the ELMy H mode

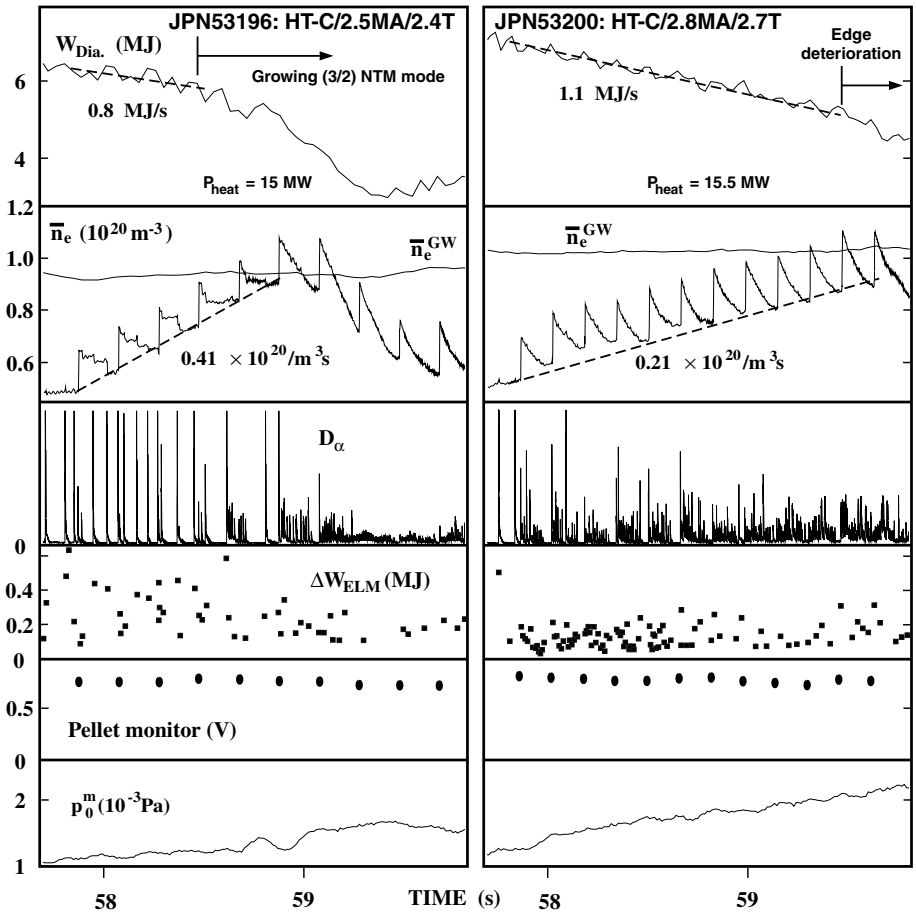

Figure 7. Comparison of pellet refuelling at 2.5 MA/2.4 T (left) and 2.8 MA/2.7 T. Operation at higher I_p/B_t is less prone to NTMs but is hampered by enhanced ELM losses. Despite a higher pellet rate (6.25 Hz instead of 5 Hz), ELM losses result in a slower density ramp-up at elevated B_t. Furthermore, stronger energy loss and parasitic gas puff occur.

phase, especially in the presence of strong pellet induced ELM bursts. Nevertheless, it was possible to increase total heating power sufficiently to avoid unwanted core NTM activity.

Using the 2.5 MA/2.4 T configuration and limiting the pellet rate to about 6 Hz, the available pumping capability was sufficient to prevent a dangerous neutral gas pressure increase even in the vertical target configuration required for good ICRH coupling. Further limitation of p_0^m and a good compromise between too strong a density ramp-up on the one hand and too long a density buildup time on the other were obtained by reducing the repetition rate. Starting with a pellet train at the full preprogrammed repetition rate, a reduced injection frequency was eventually realized by dumping some pellets. Optimization of this sequence was also performed with respect to the pellet fuelling cycle established in the vicinity of the required density while taking into account particle sustainment and energy recovery times. Typical pellet sequences were started about 2 s after the heating power had reached the 9 s maximum power plateau phase available in this configuration, when stable steady state background plasma conditions were established. Beginning with an initial series at a rate of 6 Hz for about 1 s, the rate was then reduced to 2 Hz for the remaining refuelling sequence time of up to 4 s in order to allow a reasonable density ramp-down before the heating power was stepped down. The results obtained using this optimized setting are presented in Section 4.3.

4.3. Long pulse fuelling to densities at the Greenwald level avoiding persistent confinement degradation

Applying the refuelling scenario optimized in the way described above, a successful density increase beyond the Greenwald level without significant persistent loss of plasma energy content was achieved by HFS pellet injection. This is shown in Fig. 4.3, where the temporal evolution of essential plasma parameters — energy, normalized pressure, and line averaged and central density — obtained in such a sequence are displayed along with the D_α radiation signal from the outer divertor region for ELM monitoring and the microwave pellet mass detector signal. For the example shown, a power of about 1 MW ICRH was delivered, adding to about 17 MW NBI for a total of 18 MW heating power. The initial 6 Hz pellet sequence causes the expected energy drop due to enhanced ELM activity. To allow full energy recovery, an extra pellet was dumped before entering the 2 Hz sequence. In this way the initial target plasma conditions are transformed to a higher density level even before the final pellet sequence at the reduced repetition rate starts. This is more favourable for deep pellet penetration and particle deposition, and hence improved refuelling performance is achieved. With this reduced repetition rate, the transient energy drop initiated by each pellet can be almost fully recovered before the next pellet arrives in the plasma. Nevertheless, successive

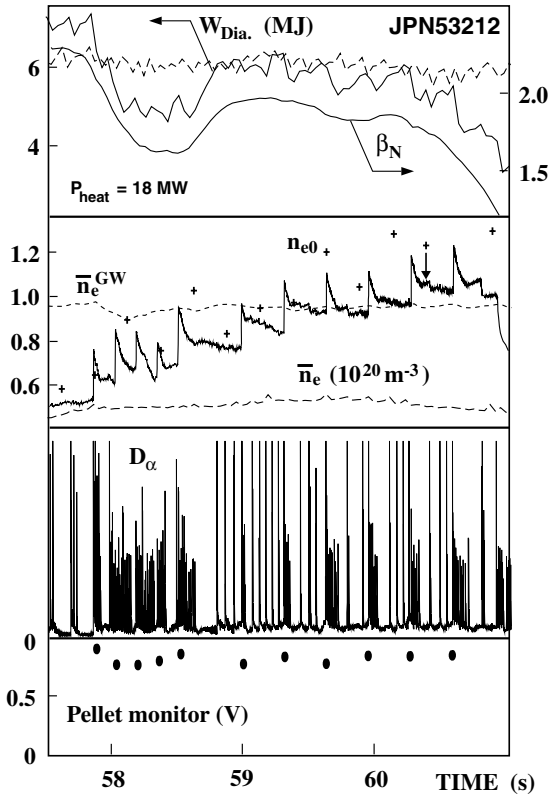

Figure 8. Optimized pellet refuelling for high performance, high density operation. Energy recovery after the initial pellet sequence and a reduced 2 Hz pellet rate in the remaining pellet sequence established refuelling cycles with gradually increasing density. Finally $\bar{n}_e > \bar{n}_e^{GW}$ is achieved while almost the same energy content is maintained that can be achieved in the reference discharge with no refuelling (dashed lines, $P_{heat} = 16$ MW).

injection gradually drives up the density further until finally the required density level is achieved. The discharge approaches its required status through refuelling cycles that show pellet driven density increases followed by short phases of strong particle and energy losses that turn into confinement recovery phases before the next pellet initiates the next density step-up. Eventually $\bar{n}_e > \bar{n}_e^{GW}$ is reached with about 6 MJ plasma energy content and β_N still above 1.8, corresponding to an H97 scaling factor of about 0.82. Finally the high performance phase is terminated by a pellet triggered (3/2) NTM, indicating that the available heating power is just marginally sufficient for this kind of operation.

Compared with a reference discharge with no refuelling with slightly less heating power (16 MW NBI), the same energy content is confined in the plasma but at about twice the particle inventory and with a much more peaked density profile. This profile shaping by the pellets is shown in Fig. 9, where density, temperature and pressure profiles are compared. The solid lines show profiles from the high density phase in the pellet refuelling experiment (taken by LIDAR systems and ECE at the time indicated by an arrow in Fig. 4.3), and the dashed lines show profiles from the reference discharge (averaged over ten profiles from the steady state phase). Pellets managed to uncouple the rather stiff relation between edge and core density usually found in scenarios where density ramp-up is produced by gas puff refuelling. At the expense of slightly

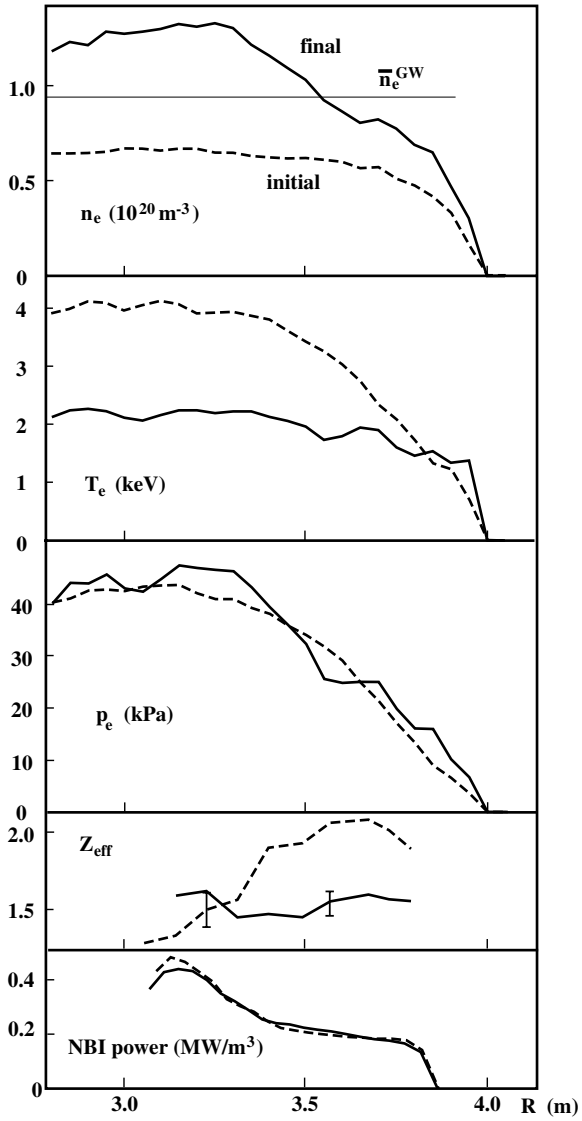

Figure 9. Density, temperature, pressure, Z_{eff} and NBI power deposition profiles for the high density phase at about 60.1 s (solid) and initial profiles (dashed).

more heating power with respect to the reference discharge, a more peaked density profile and a correspondingly flattened temperature profile are achieved, while the pressure profile is virtually identical. The slightly reduced energy confinement in the pellet discharge is due to remaining ELM losses but might also be attributed to slightly less favourable NBI power deposition profiles for the high density profile, also shown in Fig. 9. Significant reduction of the plasma impurity content is achieved, as can be seen from the Z_{eff} profiles, also shown in the figure, obtained for the phase just before pellet injection and during the high density phase.

Analysis of the safety factor and the current density profiles applying an equilibrium solver shows that there is no substantial modification by the pellets. This is because pressure and resistivity profiles remain essentially unchanged. Although pellet induced density increase reduces the temperature, its effect on the resistivity is compensated by the simultaneous reduction of Z_{eff}.

To allow an assessment of the performance achieved in the various pellet refuelling approaches, a comparison between the best performing discharges with and without gas puff refuelling in the same plasma configuration and with similar heating powers was made. The values derived for steady state phases are provided by a database [30] which, for example, shows the Greenwald fraction of the density versus the energy confinement time with respect to the ELMy H mode scaling [28]

$$\tau_E = \mathrm{H97} \times \tau_E^{H97}$$

with

$$\tau_E^{H97} = 0.029 I_p^{0.9} B_t^{0.2} P_{heat}^{-0.66} A^{0.2} R_0^{2.03} n^{0.4} \epsilon^{0.19} \kappa^{0.92} \qquad (8)$$

with A the atomic mass and ϵ the inverse aspect ratio; the units are MA, T, MW, amu, m and 10^{20} m^{-3}.

The database values plotted in Fig. 10 were obtained in experiments both with the current gas box and with the previous MKII divertor. Values from a reference gas scan [18] and the unfuelled reference discharges were added, together with the pellet data. Obviously the reference data points agree very well with the database set and the pellet refuelling can significantly enhance the accessible operational area in the plasma configuration employed. Clearly visible is the drastic confinement degradation for gas puff refuelled discharges when $f^{GW} = 0.85$ is approached, inhibiting H mode operation at the Greenwald level. On the other hand, this goal can be quite easily achieved when using pellets, as can also be seen in Fig. 4.3. From Fig. 10 it also becomes clear that the H97 scaling describes the attainable plasma energy confinement level rather well up to about $f^{GW} \approx 0.7$ but shows a growing discrepancy when $\bar{n}_e$ is increased further. This evolution, which was previously indicated by data from gas puff scans, becomes obvious in the pellet experiments. It seems that the confinement scaling changes from $\sim\bar{n}_e^{0.4}$, which is valid for low and moderate densities, to a behaviour more like $\sim\bar{n}_e^{0}$ in the high density range. The evolution of a pellet discharge in this f^{GW}–H97 diagram occurs, as already mentioned, in fuelling cycles with maximum values expanding along an almost isoenergetic contour. The short phase of strong energy and particle losses following pellet injection drives discharge parameters somewhat away from this boundary line, but the discharge then recovers to maximum performance. The amplitude of the fuelling cycle with the performance parameters used is illustrated by the spread of the data.

To illustrate the way pellets can provide more flexibility of plasma operation, the evolution of the pellet refuelling discharge is added to a diagram displaying $n_i(0) \times \tau_E$ versus central ion temperature $T_i(0)$ for various magnetic confinement fusion experiments (Fig. 11). Pellets can be used to transfer initial plasma parameters to higher $n_i(0) \times \tau_E$ values at lower temperatures.

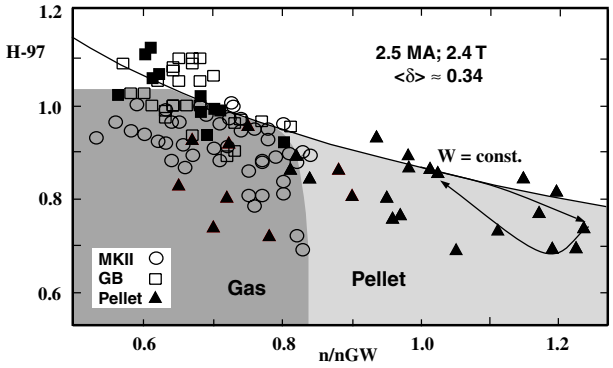

Figure 10. Extension of accessible operational area for a 2.5 MA/2.4 T HT plasma configuration by pellet refuelling shown in an f^{GW}–H97 plot. Values from the JET database for MKII (open circles) and the current gas box (open squares), as well as from reference shots (filled squares), are included. Pellet refuelling (filled triangles) allows high density operation at an elevated confinement level. In the high density range, confinement scaling seems to lose the favourable density dependence.

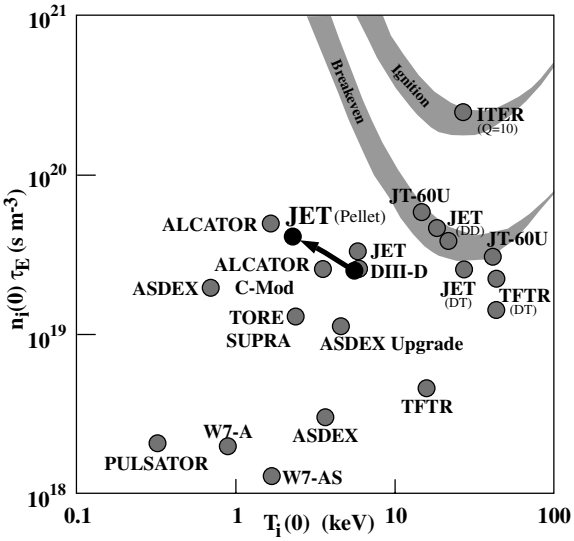

Figure 11. Evolution of a pellet refuelled shot in a $T_i(0)$–$n_i(0)\tau_E$ diagram.

5. Outlook for further improvement of pellet injection

The experiments performed during this study demonstrated the potential of pellet injection to improve the operational capabilities of a large tokamak. However, there still seems to be room for further enhancement of the pellet injection technique. The essential goal of improving pellet refuelling performance entails a further reduction of pellet imposed disadvantages, i.e. mainly post-injection losses. Therefore there is a need to realize deeper pellet penetration into the plasma. As deeper penetration results in deeper deposition and hence in a reduction of particle and energy losses in the fast density decay phase [16], pellet penetration appears to be the key to improvement of the pellet injection technique.

A closer look at the pellet penetration and deposition achieved in the experiments performed showed that pellets can approach the tangency point of the designated trajectory rather closely. Therefore the useful pellet velocity component perpendicular to the flux surfaces is drastically reduced and the penetration potential diminished. Since the regression analysis for JET data yields $\lambda_P \sim T_e^{-0.89} n_e^{-0.30} v_\perp^{0.41}$ [22], this situation can be expected to become even worse with increasing density and the associated reduced temperature. Indeed, increasing

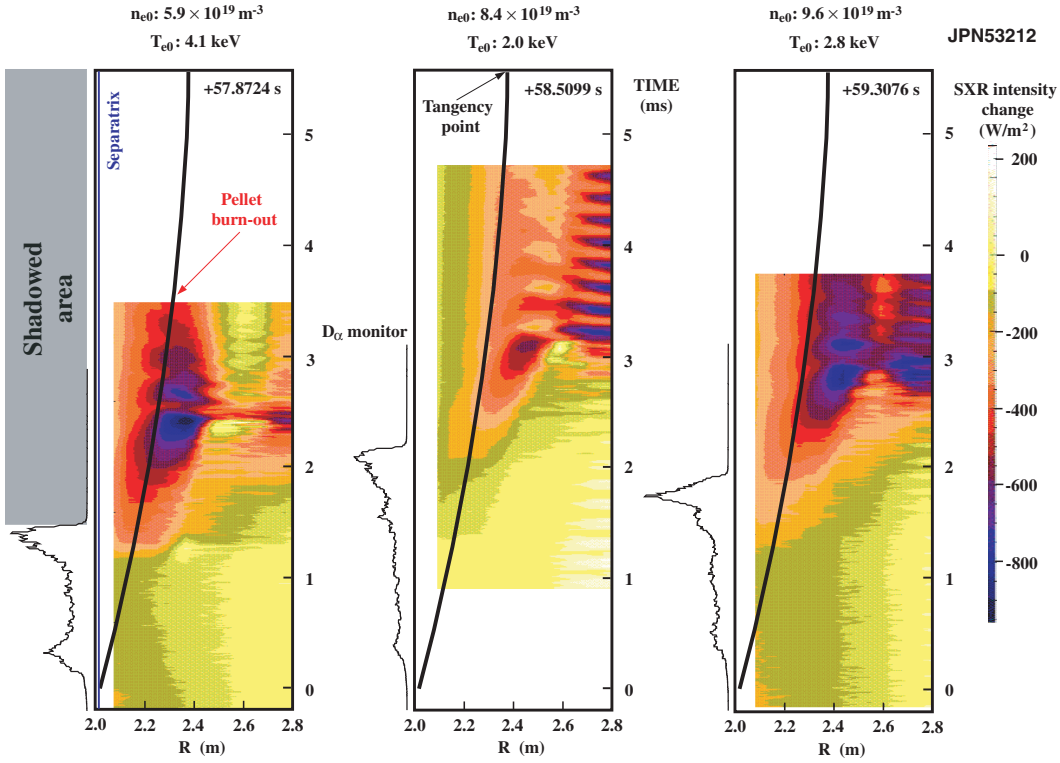

Figure 12. Pellet penetration into different target plasmas: higher densities and lower temperatures allow deeper penetration. D_α radiation is shadowed for the final part of the pellet path but indicates the entrance time. The deconvoluted SXR intensity illustrates the final part of the pellet path (solid line: trajectory up to the final tangency point adjusted for entrance time and mapped onto the horizontal midplane). HFS separatrix position, estimated pellet burn-out and tangency points are also shown.

pellet penetration and reduction of the useful pellet velocity component $v_\perp$ were found when the density was ramped up, as shown in Fig. 12. For three pellets injected during the density ramp-up sequence of JPN 53212, which has already been described, data recording for both the D_α monitor and the SXR radiation was obtained at high temporal resolution. From the D_α signals shown in Fig. 12 as well as from earlier video observations [19], it became obvious that the pellet injection path beyond about 30 cm inside the separatrix is shadowed for the observation channel. Therefore D_α signals unfortunately cannot be used to derive penetration depths but can indicate the time the pellet enters the plasma. Deconvoluted SXR profiles mapped onto the horizontal midplane axis (intensity deviation with respect to the initial profiles is shown for improved contrast) show no clear indication of the beginning of the pellet path in the plasma. However, since the ablation rates approach maximum values and thus changes of local temperature and density are strongest, SXR data show the pellet close to the burn-out point. Thus both data sets allow an estimate to be made of λ_P values. The D_α traces and SXR profile evolution plotted in Fig. 12 for the three pellets, together with the pellet trajectory mapped onto the horizontal midplane by adjusting to the start of the D_α radiation, confirm the compatibility of the two signals. As expected, for the same plasma pressure profile, pellets entering a plasma with a higher density penetrate deeper into the plasma, as can be concluded by comparing the pellets injected at 57.8724 and 59.3076 s. The pellet arriving at 58.5099 s marks the end of the initial density ramp-up sequence and thus arrives in a phase of already enhanced density but transiently reduced energy content. Consequently this pellet advances furthest along the injection trajectory, passing 80% of the distance to the tangency point. Towards the end of the pellet ablation, $v_\perp$ has shrunk to only 35 m/s.

Realizing this massive degradation of penetration potential, especially in the final part of the ablation region where most pellet particle deposition takes place, it seems that the HFS launch set-up available during this study is not yet fully optimized with respect to a maximized $\lambda_P(\rho)$, particularly when aiming at the high densities thought to be the 'natural' operational area for pellet refuelling. Since pellet approach close to the tangency point is going to take place even with the highest heating powers applied and with the currently available moderate pellet injection velocities, it becomes clear that there is little room left with the current set-up for further improvements, for example through increasing pellet mass or velocity. Therefore a technical assessment has been performed in order to find alternative injection scenarios capable of making even better use of the available penetration potential especially when operating at high plasma densities. During this assessment it was found that, owing to technical restrictions, there is only one more possible pellet launch position. Above the vessel reinforcement ring but below the supporting structures for the upper divertor, this alternative position is located about 1 m above the current exit. For both the existing and the alternative launch positions, different injection paths can be realized by a variation of the angle of the final part of the guide tube with respect to the horizontal plane. However, a close correlation exists between

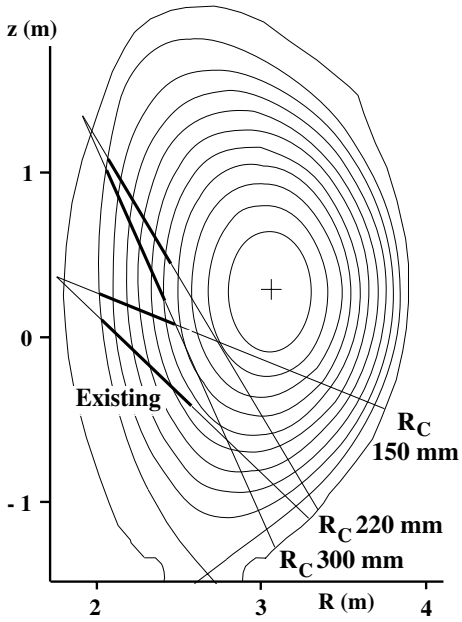

Figure 13. Typical poloidal cross-section of a plasma configuration for a high density scenario showing existing and alternative injection paths (the curvature radii R_c at the guide tube exit are indicated). Bold lines: λ_P along existing and alternative injection paths estimated using the NGS code for a typical pellet in a high density plasma, representing the expected penetration for HFS injection, with the alternative schemes yielding higher penetration potential.

the guide tube's final bend radius and the resulting injection angle. Directing the pellets more towards the plasma centre unfortunately requires a narrower bend and thus limits the maximum achievable launch speed. Thus there needs to be a compromise between a maximum geometrical penetration potential and a pellet velocity achievable for this injection path making the best use of this potential. To elucidate this, a total of four alternative schemes were analysed in more detail. The injection paths are shown in Fig. 13. For the existing lower launch position, besides the current injection set-up with a final curvature radius $R_c = 220$ mm, a version with $R_c = 150$ mm was chosen. For the alternative upper launch, two versions, with $R_c = 220$ mm and $R_c = 300$ mm, were selected, also representing different approaches with respect to velocity and geometrical penetration potential.

To allow a judgement of the capabilities available with these four injection scenarios, a comparison of penetration depths was performed using a modelling approach. In the code used, pellet erosion rates are calculated assuming the neutral gas shielding model. Despite the fact that the code only considers the shielding of the neutral cloud, uses a simple 1-D ablation geometry and assumes monoenergetic incident electrons, good agreement was found with most experiments involving LFS pellets. Therefore code results can be expected to allow a reasonable comparison of different injection paths, but absolute penetration depths may differ for HFS launch. Code runs were performed assuming plasma density and temperature profiles typical for a high density phase with good confinement, i.e. taking the experimental data from the 'final' profiles shown in Fig. 9 as well as the magnetic configuration of this discharge. For the pellet mass the typical experimental value for HFS launch of 1.6×10^{21} D atoms was adopted. Finally the maximum pellet launch velocities available for the different scenarios were assumed to follow the relation $v_P^2 \sim R_c$ found in test bed investigations [31]. Consequently, since $R_c = 220$ mm corresponds to $v_P = 160$ m/s for the type of pellet used, a value of 130 m/s was taken in the simulation of the set-up with $R_c = 150$ mm and $v_P = 190$ m/s for the case with $R_c = 300$ mm.

However, as mentioned before, HFS injection results in deeper penetration than LFS injection as represented by the code. Previous experiments indicated something like a doubled λ_P. Pellet penetrations observed in this study are also in good agreement with this value. Speculating that the scaling law $\lambda_P^{HFS} \approx 2 \times \lambda_P^{LFS}$ holds for all the scenarios, penetration depths like those shown by the bold lines in Fig. 13 are expected. In all four scenarios, pellets advance to about $\rho \approx 0.7$. In this case, improved potential for the pellet penetration could be realized using a more suitable HFS injection path. This improvement may be even greater for faster or larger pellets. Hence, beyond approaches for an improvement of the refuelling performance by changing the set-up, consideration can be given to allowing better pellet parameters using the existing set-up. To delay and mitigate losses, pellet particles must be deposited deeper inside the plasma by increased pellet velocity. Also, an increase of the pellet mass would result in an extension of the ablation profile towards the plasma centre and yield more favourable refuelling. Since the necessary upgrade of the hardware is costly and troublesome, enhancement of the pellet's intrinsic properties may be a desirable alternative approach. It was proposed to increase the yield strength of the deuterium ice by doping with small amounts of suitable materials [32]. This pellet hardening to improve mechanical stability could allow a higher velocity before significant damage occurs. Investigations of this approach have already begun in test bed runs of the novel injection set-up for ASDEX Upgrade using a pellet centrifuge launcher similar to the JET injector. First tentative results indicate a significant reduction of pellet degradation for operation in the vicinity of the critical velocity for the onset of destruction for doped pellet ice with about 1% N_2. As shown in Fig. 14, the efficiency of pellets transferred through the whole pellet guiding system at ASDEX Upgrade [16] in reasonable conditions can be improved by doping. The impurity radiation losses in the plasma imposed by such doping were estimated in an evaluation with the STRAHL code [33] to be quite bearable. Further development of this pellet hardening technique is under way, and is foreseen to improve the potential of pellet injection beyond the level achieved so far.

6. Summary and conclusions

In the investigation presented here it was demonstrated that pellet injection is suitable for long pulse fuelling to high densities in the vicinity of the Greenwald density while keeping the ELMy H mode. To achieve this goal a series of possible degradation mechanisms must be avoided. This is essential to avoid excessive edge density increase by parasitic pellet borne gas, the triggering of core MHD events, in particular NTMs triggered by pellets when the plasma is cooled too strongly, and the persisting energy losses due to pellet induced ELM losses. The boundary conditions were met by using appropriate

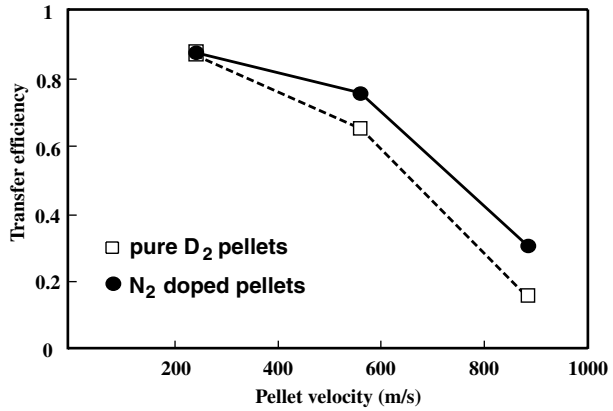

Figure 14. Transfer efficiency of cubic (2 mm)^3 pellets through the ASDEX Upgrade injection set-up for pure D_2 and for about 1% N_2 doped ice.

plasma configurations with sufficient heating power; the experiments showed, however, that available heating powers still extend only marginally beyond a critical level. Future plans to extend heating power capabilities at JET, for example in the framework of the enhancement project (JET-EP), could improve this situation.

Improvement of the pellet refuelling approach is due to the capability to break the rather stiff relation between edge and core density present in gas puffed discharges. Profile manipulations by the pellets can lead to peaked density profiles by raising the central density while keeping edge profiles almost unchanged. This capability to increase the plasma particle inventory without significant loss of confinement results in an extension of the accessible tokamak operational area. These pellet experiments confirm that the confinement scaling becomes independent of density when the density approaches $\bar{n}_e^{GW}$, as had been indicated by gas puff refuelling experiments at elevated densities [18]. With respect to the fusion relevant parameters n_i, T_i and τ_E, the pellet injection approach yields the potential for almost adiabatic movements in the operational space, raising the possibility of driving discharge parameters in regions better suitable for breakeven.

Recently, applying extreme plasma shaping, i.e. using very high triangularity, improvement of the operational parameters was achieved. In particular, the density level where the onset of confinement degradation with neutral gas density occurred was improved significantly [34]. It seems possible that the benefits achieved with HFS pellet refuelling can be combined with the advantages of these advanced shaped plasmas. In particular, pellet refuelling is expected to yield enhanced particle fuelling efficiencies compared with gas bleeding, allowing an economical use of the fuel.

The injection set-ups used up to now seem to be not yet fully optimized, especially not for the 'natural' high density operation. Further improvement seems still to be possible through better adapted injection geometries but also through intrinsically improved techniques such as pellet hardening. Moreover, pellet injection could profit from advanced plasma control, for example the use of local current drive to prevent the onset of NTMs [35]. At the moment it appears that pellets can indeed significantly enhance the operational possibilities in fusion research, for example the potential for physical investigations in an ITER-FEAT device of a given size can be extended. Ongoing efforts to improve the pellet performance by further optimization of the refuelling scenario and available pellet injection parameters may further enlarge the already available benefits.

References

[1] Shimomura Y. *et al* 2001 *Nucl. Fusion* **41** 309
[2] 1999 *ITER Council Proceedings: 1998, ITER EDA Documentation Series No 15* (Vienna: IAEA) p 148
[3] Aymar R. *et al* 2001 *Fusion Energy 2000 (Proc. 18th Int. Conf. Sorrento, 2000)* (Vienna: IAEA) CD-ROM file OV/1 and http://www.iaea.org/programmes/ripc/physics/fec2000/html/node1.htm
[4] Greenwald M. *et al* 1988 *Nucl. Fusion* **28** 2199
[5] Parks P.B., Turnbull R.J. and Foster C.A. 1977 *Nucl. Fusion* **17** 539
[6] Kaufmann M., Lackner K., Lengyel L.L. and Schneider W. 1986 *Nucl. Fusion* **26** 171
[7] Söldner F.X. *et al* 1988 *Phys. Rev. Lett.* **61** 1105
[8] Baylor L.R. *et al* 1992 *Nucl. Fusion* **32** 2177
[9] Mertens V. *et al* 2000 *Fusion Energy 1998 (Proc. 17th Int. Conf. Yokohama, 1998)* (Vienna: IAEA) CD-ROM file EX3/6 and http://www.iaea.org/programmes/ripc/physics/start.htm
[10] deKloe J. *et al* 1999 *Phys. Rev. Lett.* **82** 2685
[11] Müller H.W. *et al* 1999 *Phys. Rev. Lett.* **83** 2199
[12] Lang P.T. *et al* 1997 *Phys. Rev. Lett.* **79**1487
[13] Lang P.T. *et al* 2000 *Nucl. Fusion* **40** 245
[14] JET Team 2001 *Nucl. Fusion* **41** 189
[15] Müller H.W. *et al* 2002 *Nucl. Fusion* **42** in press
[16] Lang P.T. *et al* 2001 *Nucl. Fusion* **41** 1107
[17] Takenaga H. and JT-60 Team 2001 *Phys. Plasmas* **8** 2217
[18] Saibene G. *et al* 1999 *Nucl. Fusion* **39** 1133
[19] Jones T.T.C. *et al* 2001 *Controlled Fusion and Plasma Physics (Proc. 27th Eur. Conf. Budapest, 2000)* Vol 24B (Geneva: European Physical Society) CD-ROM file OR04
[20] Lang P.T. *et al* 1996 *Nucl. Fusion* **36** 1531
[21] Lang P.T. *et al* 2001 *Controlled Fusion and Plasma Physics (Proc. 27th Eur. Conf. Budapest, 2000)* Vol 24B (Geneva: European Physical Society) CD-ROM file P3.045
[22] Baylor L.R. *et al* 1997 *Nucl. Fusion* **37** 445
[23] Lorenzini R. *et al* 2002 *Controlled Fusion and Plasma Physics (Proc. 28th Eur. Conf. Madeira, 2001)* Vol 25A (Geneva: European Physical Society) CD-ROM file P1.2
[24] 2000 *Descriptive Analysis of 1999 Task Force P Data, Rep. JET-R(00)02* (Abingdon: JET Joint Undertaking)
[25] Bucalossi J. *et al* 2002 *Controlled Fusion and Plasma Physics (Proc. 28th Eur. Conf. Madeira, 2001)* (Geneva: European Physical Society) CD-ROM file P4.82
[26] Pitcher C.S. *et al* 2002 *Controlled Fusion and Plasma Physics (Proc. 28th Eur. Conf. Madeira, 2001)* (Geneva: European Physical Society) CD-ROM file P4.86
[27] Günter S., Gude A., Maraschek M., Zohm H. and ASDEX Upgrade Team 1998 *Nucl. Fusion* **38** 1431
[28] ITER Confinement Database and Modelling Working Group 1997 *Plasma Phys. Control. Fusion* **39** B115
[29] Suttrop W. 2000 *Plasma Phys. Control. Fusion* **42** A1
[30] Cordey J.G. *et al* 2002 *Controlled Fusion and Plasma Physics (Proc. 28th Eur. Conf. Madeira, 2001)* (Geneva: European Physical Society) CD-ROM file P3.11
[31] Lorenz A., Lang P.T. and Lang R.S. 2000 *Rev. Sci. Instrum.* **71** 3736
[32] Alexeeva L.A. and Kazeev M.N. 1990 *Paper presented at Workshop on Refuelling of Fusion Plasmas, Kurchatov Inst., Moscow (1990)*
[33] Behringer K. 1987 *Rep. JET-R(87)08* (Abingdon: JET Joint Undertaking)
[34] Ongena J. *et al* 2001 *Plasma Phys. Control. Fusion* **43** A11
[35] Zohm H. *et al* 2001 *Nucl. Fusion* **41** 197